

Article

The Effectiveness of Spraying nTiO₂ on Coating Mortars in Historical Buildings Aimed at Reducing Fungal Growth

Fernanda Lamego Guerra ^{1,*}, Caroline Giordani ¹, Lais Zucchetti ¹, Rodolfo Ribas ², Angela Borges Masuero ¹, Denise Carpena Coitinho Dal Molin ¹ and Fatima Menezes Bento ²

¹ Laboratório de Materiais e Tecnologia do Ambiente Construído (LAMTAC), Núcleo Orientado para Inovação na Edificação (NORIE), Universidade Federal do Rio Grande do Sul (UFRGS), Av. Osvaldo Aranha, 99, 7th Floor, Porto Alegre 90035-190, Brazil; caroline.giordani@ufrgs.br (C.G.); lais.zucchetti@ufrgs.br (L.Z.); angela.masuero@ufrgs.br (A.B.M.); dmolin@ufrgs.br (D.C.C.D.M.)

² Laboratório de Biodeterioração de Combustíveis e Biocombustíveis (LAB-BIO), Instituto de Ciências Básicas da Saúde (ICBS), Universidade Federal do Rio Grande do Sul (UFRGS), Ramiro Barcelos Street, 2600, Room 536, 5th Floor, Building n° 21116, Porto Alegre 90035-003, Brazil; rodolfo.ribas@ufrgs.br (R.R.); fatima.bento@ufrgs.br (F.M.B.)

* Correspondence: fernanda.guerra@ufrgs.br

Abstract: In historic mortars, the main binder used are calcitic or dolomitic lime. However, these mortars are also susceptible to the biochemical action of fungi causing undesirable changes in those materials. Nanotechnology has been investigated as a strategy to mitigate the deterioration of the cultural heritage. Photocatalysis has proven effective as an agent of degradation of organic contamination by inhibiting the recolonization of substrates affected by biological growth. This study verifies the effectiveness of a nanometric photocatalyst (nTiO₂-P25, 3% in deionized water) sprayed on the surface of simple lime–sand mortar (1:4 mass trace), typically used in historical buildings, against the growth of *Aspergillus niger* fungal isolates, inoculated with a 10⁶ spore/mL suspension. The samples were exposed to the incidence of artificial radiation of UVA light with a wavelength of 285 nm to activate the nTiO₂. We observed a reduction in fungal colonies, especially after four hours of exposure per day, reaching 100% in the staining reduction in one case. Another aspect observed was that the previous application of nTiO₂ on the mortar samples caused alterations in the morphology of the *A. niger* fungus structures, evidence of a disturbance in the growth of the colonies or even their reduction over time.

Keywords: fungal growth; historic mortar; nTiO₂ photocatalyst; *Aspergillus niger*



Citation: Guerra, F.L.; Giordani, C.; Zucchetti, L.; Ribas, R.; Masuero, A.B.; Dal Molin, D.C.C.; Bento, F.M. The Effectiveness of Spraying nTiO₂ on Coating Mortars in Historical Buildings Aimed at Reducing Fungal Growth. *Buildings* **2023**, *13*, 2751.

<https://doi.org/10.3390/buildings13112751>

Academic Editor: Ana Luísa Velosa

Received: 18 September 2023

Revised: 9 October 2023

Accepted: 29 October 2023

Published: 31 October 2023



Copyright: © 2023 by the authors. Licensee MDPI, Basel, Switzerland. This article is an open access article distributed under the terms and conditions of the Creative Commons Attribution (CC BY) license (<https://creativecommons.org/licenses/by/4.0/>).

1. Introduction

Historical buildings were generally built with a limited variety of materials, which were available in the local region, and usually consisted of stones, bricks, wood, and traditional mortars [1–4]. These materials are frequently susceptible to alterations caused by abiotic and biotic environmental factors [1,3,5] and by the passage of time itself. Biological agents, which are naturally present in the environment, are among the main deterioration factors.

Biodeterioration produces undesirable alterations in buildings, and can be caused by bacteria, fungi, algae, and/or lichen, influenced by environmental conditions, chemical factors, and the nature of the substrate [6,7]. Kirthika et al. [8] adds that biodeterioration results in compromising of the structural materials' integrity, causing adverse effects on economic and social well-being. Jiang et al. [9] mention that when there is sufficient availability of nutrients, energy, and organic carbon sources, considering the environmental microclimate, referring to humidity and temperature, filamentous fungi can colonize and grow in concrete structures, affecting the physical and chemical properties of cementitious materials. The authors mention the main species of filamentous fungi that colonize and

cause the biodeterioration of cementitious materials: *Fusarium oxysporum*, *Aspergillus niger*, and *Cladosporium sphaerospermum*.

According to Beimforde [10], microorganisms can interact with materials in three main ways: the material may be decomposed by enzymes and used as a source of nutrients by microbial associations; microorganisms may excrete metabolic compounds, such as inorganic and organic acids that interact with the mineral compounds of the material, causing dissolution and discoloration; and the material can be damaged by physical (mechanical) forces due to the growth of microorganisms. Harding et al. [11] mention that fungi are a type of microorganism particularly well-adapted to growth on different surfaces, mainly due to their absorptive way of obtaining nutrients, their ability to secrete extracellular enzymes that digest complex molecules and, finally, their apical hyphal growth, through filaments (hyphae). Traces of organic matter can be present in construction materials, including organic contamination in fine aggregates or additions and additives in the fresh mix. Once the organic matter is absorbed, the cellular structure of the filamentous fungi allows its transport to the tip of the hypha, allowing the release of organic acids that modify the physical and chemical properties of the concrete and the extension of the fungus in the contaminated matrix. This behavior is unique to filamentous fungi and allows them to explore and grow in environments unsuitable for colonization by single-celled organisms such as bacteria [8].

Jiang et al. [9] highlight that the mechanisms identified as responsible for the fungus-influenced degradation of mortar substrates include the formation and leaching of soluble salts produced by the reaction of organic acids secreted by fungal cells on the carbonated matrix of concrete; the expansion due to the formation of insoluble calcium salts (Ca), such as calcium citrate, from the reaction with organic acids secreted by fungi; crack development caused by the ettringite formation from the secretion of the keratinase enzyme and amino acids; and the potential mechanical attack by fungal hyphal growth and expansion into solubilization zones and cracks.

The main binders used in historical mortars are magnesium and calcium carbonates; hence, these mortars are also susceptible to the biochemical action of fungi, depending on the availability of organic nutrients and the presence of other factors that favor their growth, such as water and adequate temperature and pH. Therefore, as stated by Burford, Fomina, and Gadd [12], fungi are considered important agents of deterioration of carbonate minerals. Calcium ions (Ca^{2+}) are essential for fungal apical growth and are required in high concentrations at the tip of the hypha. When the ideal concentration is reached, hyphal extension is stimulated and hyphal branching is inhibited. According to Jiang et al. [9], concrete, like historic mortars, is a high-Ca environment that provides a rich source of Ca^{2+} for mold growth. Indeed, Ca^{2+} plays a prominent role in the attack of organic acids on carbonate-based substrates, altering the physicochemical properties and promoting fungal extension in the material matrix.

According to Verrecchia [13], these microorganisms, through the development of the mycelium, can form an arrangement of filaments in the substrate. As a way of obtaining Ca^{2+} for their metabolism, filamentous fungi have developed the ability to concentrate those ions in their filaments in the form of calcium oxalate salts or calcium carbonate, inside or outside their membrane. In favorable conditions of humidity and temperature, fungal growth and sporulation increases the concentration of spores, especially in indoor environments, increasing the risk of biodeterioration [9,14,15].

Coffin et al. [16] describe five antimicrobial agents widely applied in industry, including building materials: triclosan (2,4,4'-trichloro-2'-hydroxy-diphenyl-ether, CAS #3380-34-5), silver-impregnated zeolite and silver nanoparticles (nanosilver), copper, quaternary ammonia compounds, and formaldehyde donors. The authors address aspects of antimicrobial resistance developed when microorganisms are not killed and undergo mutations over time. Potential human and environmental health impacts promoted by these additives could include antibiotic resistance. The emergence of antimicrobial additives in ecosystems also needs to be further investigated and clarified.

Nanotechnology applied to different areas in the field of materials conservation has been investigated as a strategy to mitigate the deterioration of the cultural heritage [17–26]. The use of nanometric photocatalysts, such as nTiO₂, has been attracting the interest of scientists for several decades. According to Fujishima et al. [27], photocatalysis is generally understood as the acceleration of photochemical reactions on solid surfaces, usually semiconductors. In this process, at least two reactions occur simultaneously: oxidation, through the generation of holes, and reduction, through the photogeneration of electrons. Photocatalysis has proven effective as an agent of degradation of organic contamination by inhibiting the recolonization of substrates affected by biological growth [28]. For La Russa et al. [29], nTiO₂ is useful not only in the decomposition of a wide range of organic compounds, but it can also be used against several microorganisms, including bacteria, fungi, and even viruses. According to those authors, the process involving microorganisms happens through the competition between the recombination (in nanoseconds) of photo-excited charge carriers, electrons and holes, and their transference to the interior of the cells. TiO₂ has aroused interest in its application in the construction industry due to its self-cleaning, air depolluting, and antimicrobial properties in cement-based materials [30,31]. Jędrzejczak et al. [32] added titanium oxide, especially the anatase variety, to a cementitious matrix substrate, observing an improvement in the antibacterial properties of the composite. Castro-Hoyos et al. [33] argue that the interactions between TiO₂-based materials and the cell walls of microorganisms bring benefits for their control and prevention. They add that in laboratory tests, inactivation depends on the characteristics of the microorganism and that it is possible to reproduce standardized protocols for sample preparation, allowing real effects. Another interesting aspect highlighted by the authors corresponds to the benefit to biodiversity, since new sustainable technologies using TiO₂ aim to prevent the proliferation of microorganisms. Prevention rather than eradication is the crucial strategy to regulate and control their development on different substrates.

With regard to antimicrobial properties, although laboratory studies report the inhibition of microbial growth using cementitious materials treated with TiO₂, scaled tests are necessary to increase the photocatalytic activity of TiO₂ for different microorganisms, considering its high diversity, as well as verifying the durability of the photocatalyst on substrates; these are still concerns in the development of so-called cement-based antimicrobial materials [7].

The aim of this study is to verify the effectiveness of the nanometric photocatalyst (nTiO₂-P25, 3% in deionized water) sprayed on the surface of simple lime sand mortar (1:4 mass trace), typically used in historical buildings, against the growth of *Aspergillus niger* (*A. niger*) fungal isolates, inoculated with a 10⁶ spore/mL suspension. The samples were exposed to the incidence of artificial radiation of UVA light with a wavelength of 285 nm to activate the nTiO₂. Subsequently, the samples were monitored for approximately seven months, assessing the parameters of color and lighting variations with a spectrophotometer, the morphological structures through a stereoscopic magnifier, and photographic images through the use of the open-source software ImageJ 1.53k.

2. Materials and Methods

2.1. Fungi and Preparation of the Spore Suspension

The *A. niger* isolates (Figure 1) were identified using the molecular method of DNA extraction with PCR from the collection made at the historical building analyzed at a previous stage, and discussed by Guerra et al. [34]. Thereafter, a suspension was prepared using the selected isolates at a concentration of 10⁶ spores/mL, according to the protocol used at LAB-BIO of the Basic Health Sciences Institute of the Federal University of Rio Grande do Sul (Instituto de Ciências Básicas da Saúde-ICBS-UFRGS). Kaur and Singh [35] point out that spore density plays an important role in the general integrity of the biofilm structure. According to those authors, the inoculum selected for this study is considered high-density. For the selection of the isolate used in this study, the researchers considered both the frequency with which it was identified in previous analyses, and the color of

the colonies, to facilitate the readings with the colorimetric method. Figure 1 shows the morphological aspect of the *A. niger* colony, as well as the images obtained through optical microscopy and stereoscopic magnifier.

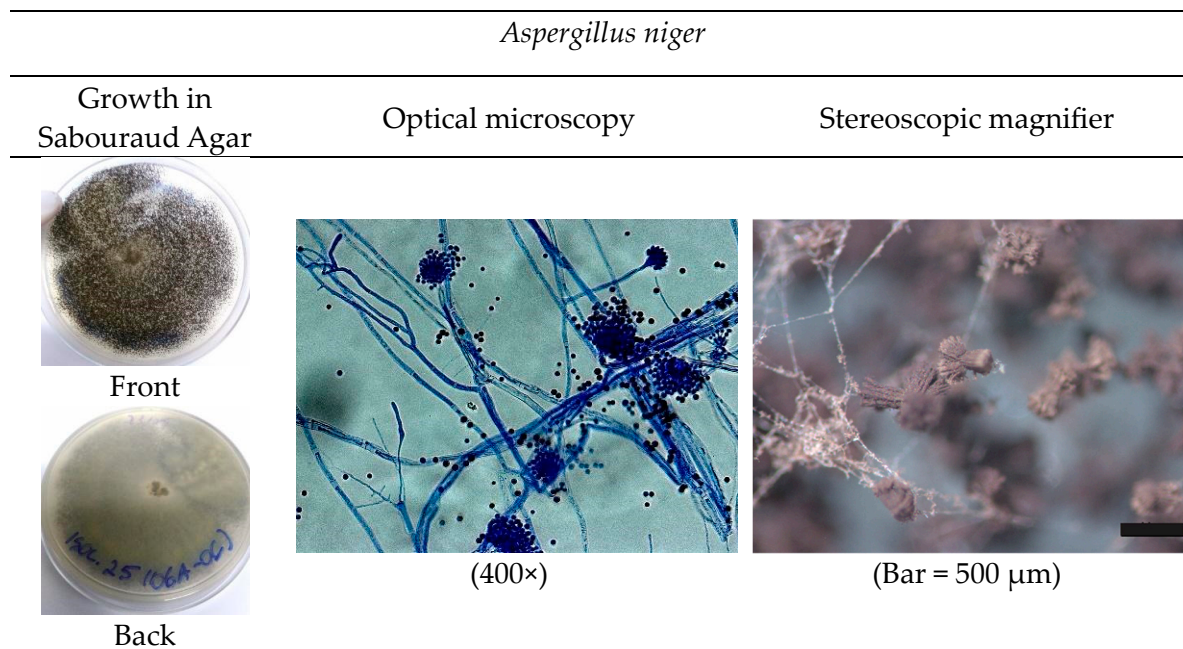


Figure 1. Aspect of *Aspergillus niger* isolate selected to study.

To perform the experiment, the fungus was cultivated in glass vials sterilized in the autoclave and sealed with a screw top, containing 10 mL of Sabouraud Dextrose Agar medium, solidifying in a tilted position to offer a larger growth area for the colonies. Approximately 3 mL of 0.01% Tween® 80 sterile solution [22] was added, and the vials were manually shaken to release the spores. The spores were counted in a Neubauer chamber and the correction for the concentration was previously determined (10^6 spores/mL).

All the samples, both those with the application of photocatalyst and those without it, were inoculated with 1 mL of 10^6 spores/mL suspension, considering 6 repetitions.

2.2. Experimental Design

This section presents the description of the experiment's stages: molding the mortar samples, curing and superficial treatment of the samples with $n\text{TiO}_2$, application of the *A. niger* inocule, and monitoring of the variation of color over time, as well as an analysis based on the images obtained from the samples. The flowchart in Figure 2 indicates the sequence of stages followed.

2.3. Molding and Curing the Mortar Samples, and Application of $n\text{TiO}_2$

The composition and trace of the samples used in this study were based on a previous study performed on a historical building from the early twentieth century in the city of Porto Alegre-RS, Brazil. The building, named Casa Godoy (1907), coordinates ($30^\circ 01' 45''$ S; $51^\circ 13' 00.77''$ W), is representative of the constructive typology of historical buildings, as described and analyzed by Guerra et al. [34].

The binder used was calcitic lime, with a calcium hydroxide concentration range between 89 and 95%, molecular weight of 74.09 g/mol, pH of 12.6 (saturated solution, temperature 20 °C), and fusion point of 580 °C, according to the manufacturer's specifications. The unit mass and the specific mass determined were $0.55 \text{ g}\cdot\text{cm}^{-3}$ and $2.306 \text{ g}\cdot\text{cm}^{-3}$, respectively. The sand used, which was quartz sand with a medium fineness modulus (3.6), was sieved, washed, and dried in the oven at 100 °C, following the granulometric

distribution in Guerra et al.'s [34] characterization data for historical buildings. Lime putty matured for 15 days was used in the mix.

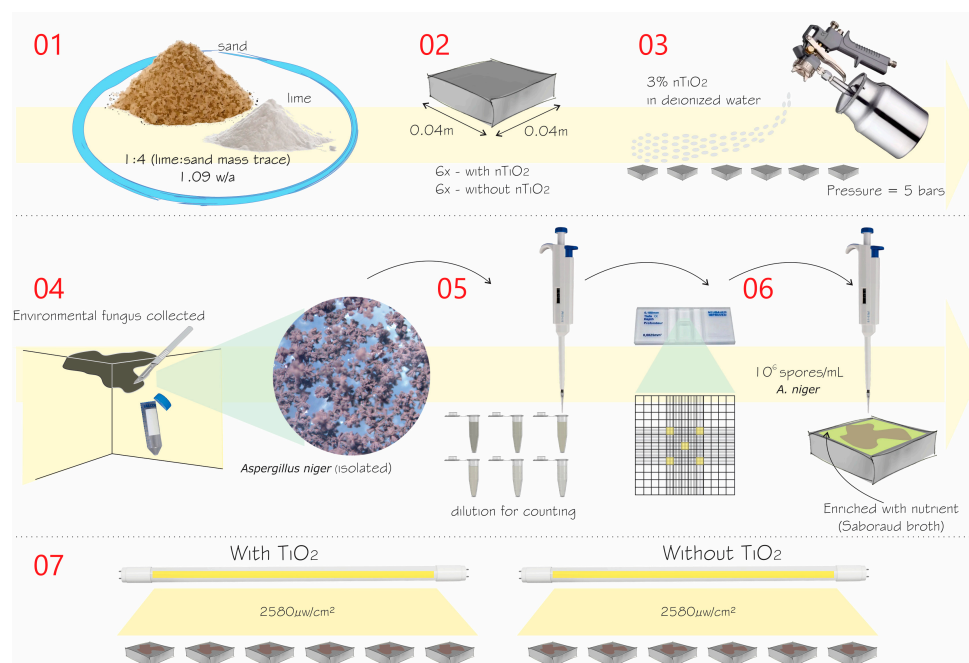


Figure 2. Flowchart of sample production steps. (01) materials for mortar composition; (02) mortar sample 0.04 × 0.04 m; (03) application of 3% TiO₂ in deionized water with a pressure gun; (04) collection and isolation of filamentous fungi; (05) serial dilution to count spores of the *A. niger*; (06) Neubauer chamber counting and application of suspension to the sample; (07) exposure of samples to UVA light.

The mortar used in the tests had a 1:4 binder aggregate proportioning in mass (lime:sand, dry materials), the most frequent value found by Guerra et al. [34], and a water/binder ratio of 1.09. The mortar samples were characterized in the fresh state as to their consistency index, according to NBR 13276 [36], resulting in 252 mm; bulk density in the fresh state, and content of entrained air, according to NBR 13278 [37], showing 1970 kg/m³ and 0.93%, respectively. In the hard state, at 90 days, the features evaluated were compressive and flexural strengths, according to NBR 13279 [38], showing 0.53 MPa and 0.51 MPa; capillary water absorption, as in NBR 15259 [39], 7.57 g/dm².min.^{1/2}; dynamic modulus of elasticity, according to NBR 15630 [40], 5542.54 MPa; and bulk density, according to NBR 13280 [41], 1802.40 kg/m³.

To evaluate the colonization of fungal isolate, samples measuring 4 × 4 × 1 cm were cast in acrylic molds coated with plastic film. After demolding, the samples were placed in a chamber with 5% CO₂ and 80% RH for a 10-day period, until carbonation was completed, as suggested in the method proposed by Shirakawa et al. [42]. This process is essential to reduce the samples' pH, encouraging biological growth, which is necessary for the performance of the analyses. The degree of carbonation was verified through a test using phenolphthalein (1% in ethyl alcohol P.A. 95%) as a pH indicator. The suspension to be applied contained Aeroxide[®] TiO₂ P 25, at 3% concentration in deionized water. This value was determined based on rheological and visual tests using a stereoscopic magnifier. To reduce the agglomeration of particles, agitation was done with an ultrasonic probe for 180 s, using a 500-watt ultrasonic processor Sonics[®] with an amplitude of 20%.

The suspension was applied with a pressure paint spray gun (paint gun HVL P 1.5 mm 600 mL Gravity PUMA-AS1105) in two transversal coats, with a 24 h break between applications. The gun was connected to an air compressor, and the pressure, measured with a barometer, was set at 5 bars. One lot not sprayed with nTiO₂ was set aside to be used as control in the analyses.

After the application and drying of the photocatalyst, all the samples were carefully packed in bags, put in the autoclave, and sterilized at 121 °C for 15 min. Subsequently, to ensure that the analysis with the spectrophotometer would be performed always at the same reading point, the samples were individually fastened with double-face tape to lidded acrylic containers previously sanitized with a solution of hypochlorite and 70% ethyl alcohol to avoid any contamination. Finally, the containers were closed and placed in an air-conditioned chamber with 80% RH for at least 72 h, as suggested by Shirakawa et al. [43].

A liquid nutritional medium (Sabouraud Dextrose Broth) was used to enrich the mortars, prepared as suggested by Shirakawa et al. [24]. The procedure consisted in pipetting 4 mL of the nutrient in each of the samples in four separate doses of 1 mL each, allowing total absorption through the surface, without any overflow.

2.4. Instrumentation of the Biochemical Oxygen Demand (BOD) Incubator and Disposition of the Samples

The equipment used for the performance of the analysis in controlled conditions of RH, temperature, and incidence of light was a Biochemical Oxygen Demand (BOD) incubator with total capacity of 340 L, internal dimensions of 1.51 × 0.53 × 0.44 m, temperature range from 5 to 55 °C, precision of 0.3 °C, and a compressed air laminar flow ventilation system.

The equipment was modified for the installation of two black light 24w-PL-L 24 W/10 4P lamps, connected with a photoperiod control system, to provide light incidence in the UVA wavelength (364–384 nm) in pre-determined time cycles, starting at 1 h/day exposures, increasing to 2 h/day and up to 4 h/day for a total period of 211 days (approximately 7 months) of experiment, as schematically shown in Figure 3.

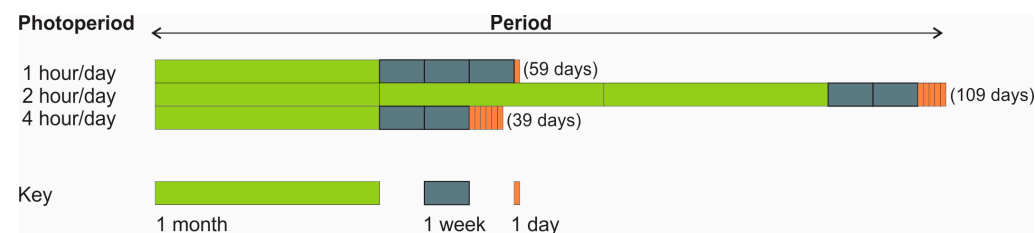


Figure 3. Period of exposure to UVA irradiation for each photoperiod.

For the maintenance of the necessary RH for the evaluation of the growth of the fungi under study, a tank present at the bottom of the equipment was filled with 30 L of distilled water. A data logger with an RH and temperature sensor was fastened to the interior of the equipment's door to allow constant recording of the microclimate, every 30 min during the experiment.

The samples were placed in the interior of the BOD so that they would all be exposed to light at 30 cm from the lamps, which presented an average UVA irradiance of 2580 $\mu\text{w}/\text{cm}^2$. The luminous intensity was regularly determined with the aid of a UVA light meter (Instrutherm), to verify the constancy of light incidence during the 211-day incubation period.

2.5. Analysis of the Samples' Light Coordinates with a Spectrophotometer

One of the methods used to verify the effectiveness of the studied photocatalyst against fungal growth consists in measuring the colorimetric variation over time. A Konica Minolta CM 2500 d portable spectrophotometer was used for that purpose. This method allows the determination of the chromatic coordinates based on the Commission Internationale de l'Éclairage (CIE) and is used in several studies with similar aims to this one [28,44–48].

This system allows the tridimensional expression of the color space in $L^*a^*b^*$ coordinates, where:

- L^* corresponds to luminosity;
- a^* corresponds to the coordinates of the colors red/green, with “+a” indicating red and “-a” indicating green;

- b^* corresponds to the coordinates of the colors yellow/blue, with “+b” indicating yellow and “-b” indicating blue.

Color variation over time (ΔE) is expressed as in (Equation (1)), according to CIE S014-4/E:2007, Colorimetry Part 4: CIE 1976 $L^*a^*b^*$ Color Space, described by Ruot, et al. [49] and Pozo-Antonio and Dionísio [28].

$$\Delta E = \sqrt{\Delta L^{*2} + \Delta a^{*2} + \Delta b^{*2}} \quad (1)$$

where:

ΔE = color variation over time

$\Delta L^* = L_t^* - L_0^*$

$\Delta a^* = a_t^* - a_0^*$

$\Delta b^* = b_t^* - b_0^*$

t = final time

0 = initial time.

The measurements of coordinates L^* , a^* , and b^* were made in specular component included (SCI) mode, with the light beam emitted through a fixed 8 mm opening, diffuse illumination system, 2 xenon flashes, 10 nm wavelength interval, as stated in the manufacturer’s specifications, and used by Pozo-Antonio and Dionísio [28].

Over time, 10 measurements were made for the samples in the BOD, as described in Table 1. The table also presents the duration of the interval between measurements 1 and 5 (before the UVA light was activated) and 6 and 10 (after the lamps were turned on).

Table 1. Range of measurements with spectrophotometer.

	Interval	Description	Time of UVA Light (Days)
Measurement 1 (M1)	52 days	Carbonated samples (with and without nTiO ₂), before nutritional enrichment. Date of application of the nutrient. Sabouraud Broth (4 mL per sample) and placement in BOD for acclimatization.	Zero
Measurement 2 (M2)		Samples with nutrient (acclimatized in the BOD), before inoculation with the isolates.	Zero
Measurement 3 (M3)		Immediately after inoculation (fresh samples).	Zero
Measurement 4 (M4)		Placement in the BOD (without turning on the lamp).	Zero
Measurement 5 (M5)		Before turning on the lamp. Date of light activation (photoperiod 1 h/day).	Zero
Measurement 6 (M6)	211 days	7 days after light activation (photoperiod 1 h/day).	7
Measurement 7 (M7)		30 days after light activation (photoperiod 1 h/day).	30
Measurement 8 (M8)		50 days after light activation (photoperiod 1 h/day). Date of the increase of the photoperiod to 2 h/day.	50
Measurement 9 (M9)		101 days after light activation (photoperiod 2 h/day). Date of the increase of the photoperiod to 4 h/day.	101
Measurement 10 (M10)		211 days after light activation (photoperiod 4 h/day).	211

Three readings were done for each sample. To ensure that observation of the alterations over time were always at the same point of measurement, a template was made to allow

positioning the equipment always at the same spot as the initial measurement. To avoid, as far as possible, any contact of the equipment with the growth surface, the researchers used a disposable Petri dish covered with black duct tape, where they made holes with a diameter compatible with the light emissions from the spectrophotometer. In the interior of the Petri dish, partitions were placed to allow the placing of the samples, restricting their lateral movement during measurements. The samples were covered with the template without any contact with the upper surface, leaving exposed only the three openings for the positioning of the spectrophotometer, fixing the reading points on those openings.

Figure 4 schematically shows the time interval between the measurements.

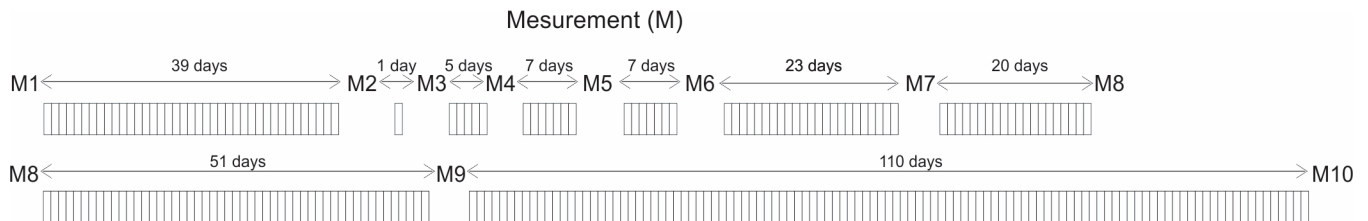


Figure 4. Time interval between spectrophotometer measurements.

Figure 5 shows the locations of diameters 1, 2, and 3 assessed in the sample, the template made for the measurements with the locations of the measurement points, and the spectrophotometer used.

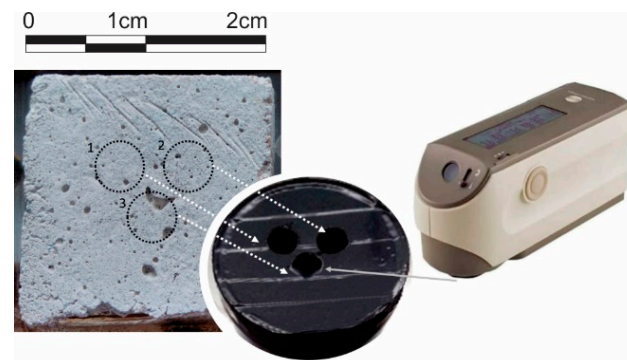


Figure 5. Schematic representation of the spectrophotometer positioning for measurement at pre-determined points in a sample.

2.6. Analysis of the Photographic Images

Throughout the duration of the experiment, and at each spectrophotometer reading, photographic images of the entire samples were obtained for subsequent analysis with image processing software. ImageJ [50] software was used to quantify the fungal growth areas for the different proposed configurations in a complementary way to analysis by spectrophotometer. This software offers a plugin, Threshold, in which the binarization of the images in 8 bits is performed, using several global limit methods (derived from histograms). The images were previously treated to present the same quantity of pixels, thus allowing a quantitative comparison of the growth area for the entire samples. The results are presented in black and white scales with their respective pixel intensities.

2.7. Analysis on Stereoscopic Magnifier

At the end of the experiments, the samples were analyzed using a Zeiss Stemi 508 doc Stereomicroscope, with up to 100× magnification. Points of growth of the fungal isolate on the mortar samples' surfaces, with and without the application of nTiO₂, were selected with the aim of making a visual comparison of the morphological structures.

3. Results and Discussion

The results and discussions of each stage of the study are presented below.

3.1. Microclimate Monitoring in the BOD

The temperature and relative humidity values were recorded inside the BOD during the experiment. The average RH recorded was 76.85%, and the average temperature, 25 °C. However, for approximately 52% of the recording time, the RH was above 80%, as shown in Table 2, and for only 0.82% of the time was it below 30%. It should be noted that in the periods when the lamps were on, the temperature inside the BOD increased, with a consequent reduction in RH, similarly to what occurs in natural conditions of exposure to solar radiation, resulting in constant oscillation of the microclimate. The maximum temperature recorded was 36 °C. Table 2 shows that during approximately 60% of the time, the temperature ranged between 25 °C and 30 °C.

Table 2. Percentage of occurrence of RH and temperature in the BOD during the test.

	Relative Humidity (RH)				
	<60%	Between 60–70%	Between 70–80%	Between 80–90%	>90%
Occurrence (%)	9.8	8.5	26	52.7	3
	Temperature (°C)				
	Between 22–25	Between 25–30	Between 30–35	>35	
Occurrence (%)	33.74	60.63	5.55	0.08	

Sedlbauer [51] presents minimum, optimum, and maximum temperature and relative humidity values for *A. niger* spore germination and mycelium growth, indicating 10 °C, 35 °C, and 50 °C for minimum, optimum, and maximum temperature, and 77% and 98% for minimum and maximum RH, respectively, for spore germination; and 6 °C, 37 °C, and 47 °C for minimum, optimum, and maximum temperature, and 76% and 98% RH, respectively, for mycelium growth. Thus, with regards to the microclimate inside the equipment throughout the experiment, for the RH values, the minimum percentage necessary was achieved both for sporulation and for spore germination of *A. niger* (77% and 76%, respectively) during most of the experiment's time. The temperature presented values between the minimum and maximum ranges, but it was predominantly below the optimum values of 35 °C for sporulation and 37 °C for germination. However, that did not hinder the growth of the samples, allowing the detection of fungal growth.

3.2. Color Variation in the Samples Inoculated with *A. niger*

As the measurements were always performed at the same locations in each of the samples in the different proposed configurations, the evolution of the characteristics read point by point by the spectrophotometer always occurred in relation to the initial reading on the same specimen. Although the inoculation of the isolate in the mortar substrates followed the same procedure, with strict control of the inoculated volume and spore counting, the biological growth on the surfaces did not occur in a uniform manner. Burford et al. [12] mention that the direction of fungal growth is influenced by the presence of grooves, ridges, and pores on the solid substrate, as well as by properties related to weakened mineral surfaces. They also point out that the penetration of fungal hyphae in the microstructure of coating mortars, observed on an electronic microscope, demonstrates their correlation with the cracking and decay of some areas of surface coating. Hence, the pre-setting of the reading points hindered the obtention of some results, since, in some of the samples, fungal growth occurred outside the pre-set area.

Out of a total of 12 samples inoculated with the *A. niger* isolate, six of them with the application of nTiO₂ and six without it; only three with the photocatalyst and two without it showed effective colony growth. Figure 6 shows growth in the samples where

the photocatalyst was applied, considering measurement 5 (before activating the UVA lamp) and the subsequent measurements, with the different photoperiods, until the final measurement (M10), when the experiment was concluded.

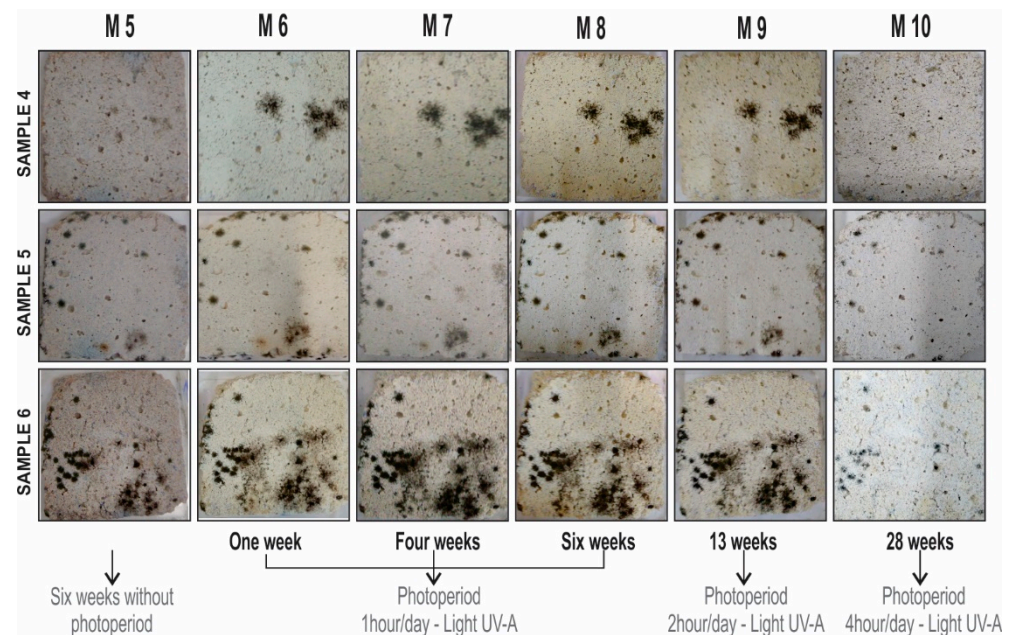


Figure 6. Evolution of the samples inoculated with *A. niger* with application of nTiO₂.

In samples 4, 5 and 6, which were superficially sprayed with nTiO₂ (Figure 6), the development of colonies starting from measurement M5 (before the lamps were switched on) was detected, developing until their maximum growth, perceptible by visual evaluation in measurement M7, with a photoperiod of 1 h/day. Between measurements M8 and M9, there was a slight reduction in the colonies, mainly in sample 6. In measurement M10, after the photoperiod was increased to 4 h/day for 15 weeks (~3 months), an effective reduction of *A. niger* fungus was detected in all three samples.

As for the cases without the application of the photocatalyst (Figure 7), in sample 12, the colonies present a barely visible initial growth, which remains practically constant until measurement 10. Sample 11 presented the growth of well-defined colonies across its surface. It is notable that, even with the incidence of UVA light, little change was detected in the development of the colonies up to the final measurement, M10.

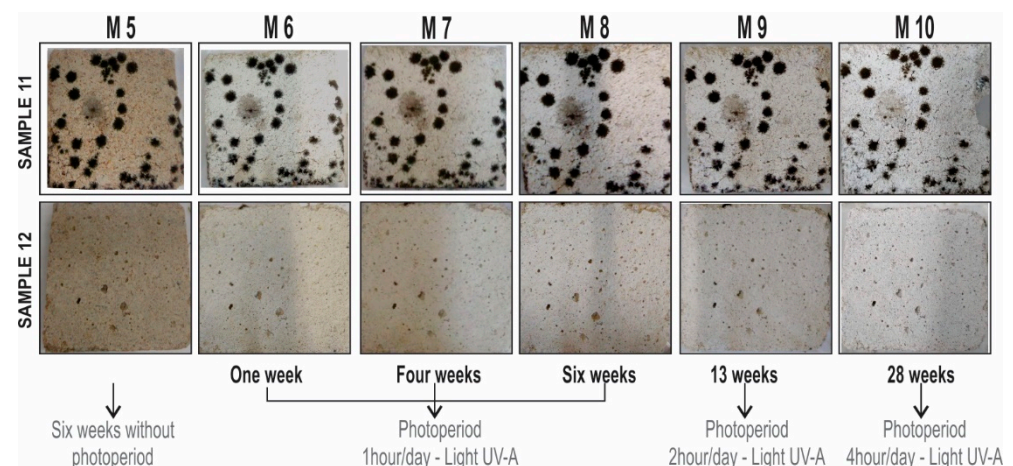


Figure 7. Evolution of the samples inoculated with *A. niger* without nTiO₂.

With the purpose of making a quantitative evaluation of the color alterations on the surface, the researchers observed the values obtained for the parameters luminosity L^* (Figures 8 and 9), coordinates a^* (variation in the red-green color spectrum), and coordinates b^* (variation in the blue-yellow color spectrum) for each of the three readings points in each of the samples, considering the presence or absence of the photocatalyst.

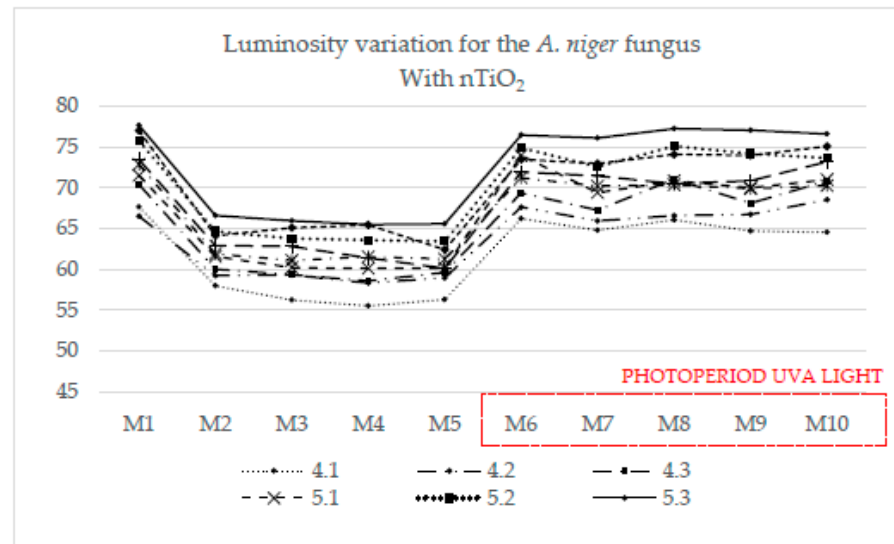


Figure 8. L^* Luminosity values for the *A. niger* fungus with nTiO₂.

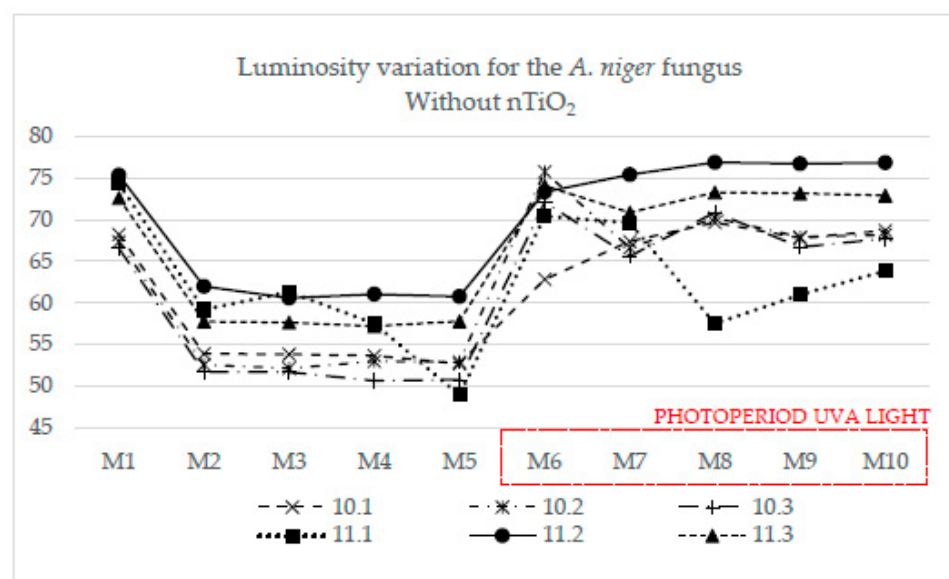


Figure 9. L^* Luminosity values for the *A. niger* fungus without nTiO₂.

Measurement M1 corresponds to the first reading, made before the application of the nutrient and the inoculum. The samples with photocatalyst (Figure 8) presented minimum luminosity of 66.53 and maximum of 77.66, with an average value, among all samples, of 73.58. In turn, the samples without the photocatalyst (Figure 9), presented minimum and maximum values of 66.55 and 75.37, respectively, with an average of 70.75 for the first measurement (M1). The samples with application of the photocatalyst presented, on average, greater luminosity due to the white coloration of the nTiO₂, which covered the surface, including the siliceous aggregates, which are a light chestnut color.

Measurement M2 shows the readings of the samples immediately after the application of the nutrient medium. Hence, the samples with the application of the photocatalyst

(Figure 8) presented a minimum luminosity of 57.99, maximum of 66.61, and average of 62.12, corresponding to a luminosity reduction of 15.57% compared with the average luminosity values. The samples without photocatalyst (Figure 9) presented a minimum luminosity of 51.69, maximum of 61.99, and average of 56.18. The reduction in relation to the average luminosity value was 20.59%.

Reading M6 was performed seven days after the 1 h/day photoperiod of radiation was activated. The values in Figures 8 and 9 show that until measurement M6, the samples generally presented a gain in luminosity. However, at M7, after 30 days of the 1 h/day photoperiod, the luminosity starts to decrease and, consequently, the maximum biological growth of most samples occurs. This behavior persists until measurement M8, except for a measurement point of sample S11 (11.1), Figure 9, which shows a drop in luminosity due to the accentuated fungal growth at this measurement point. Considering measurement M9, where the 2 h/day photoperiod has already been activated, it is possible to detect a start in the reduction of luminosity up until the final measurement, M10. There is greater luminosity gain in the samples with nTiO₂ compared with those without, except for sample S11.1 (Figure 9), which shows a tendency to gain luminosity, although at values below that of the other samples with the photocatalyst.

Table 3 shows the color variation data (ΔE^*), and Table 4, luminosity variation (ΔL^*) and coordinates a^* and b^* (Δa^*) and (Δb^*) for the samples with and without the photocatalyst, starting from the initial measurement (M1) up to the measurement with the maximum colony growth (M7) and, subsequently, the initial measurement (M1) compared with measurements M8, M9, and M10.

Table 3. Color variation over time of samples with and without application of nTiO₂.

		ΔE^*									
Sample		(M2-M1)	(M3-M1)	(M4-M1)	(M5-M1)	(M6-M1)	(M7-M1)	(M8-M1)	(M9-M1)	(M10-M1)	
With n TiO ₂	S4	4.1	9.805	11.554	12.236	11.469	5.772	9.170	10.675	8.001	6.024
		4.2	7.459	7.413	8.236	7.683	5.855	8.803	10.737	7.653	5.107
		4.3	10.497	11.178	11.892	10.872	5.653	9.413	10.455	6.860	2.470
	S5	5.1	10.108	11.419	11.495	11.465	3.940	3.824	2.785	2.548	1.174
		5.2	11.179	12.050	12.203	12.373	4.156	4.924	3.481	2.968	2.540
		5.3	11.221	11.889	12.238	12.173	3.336	3.286	2.480	1.791	1.357
	S6	6.1	11.032	11.821	11.375	11.639	4.641	7.134	7.942	7.192	3.878
		6.2	10.610	10.679	12.078	13.352	5.040	7.884	8.043	6.391	3.114
		6.3	12.960	11.989	11.615	14.625	4.982	5.870	5.427	4.533	2.445
Without n TiO ₂	S10	10.1	15.324	15.290	15.325	16.314	5.585	2.672	2.299	0.763	0.589
		10.2	15.928	16.198	15.446	15.384	8.446	2.237	3.148	0.669	1.060
		10.3	15.837	16.011	16.961	16.668	5.547	2.238	4.569	0.337	1.322
	S11	11.1	15.437	13.382	17.464	25.551	3.976	4.735	16.991	13.425	10.571
		11.2	13.881	15.122	14.693	14.923	2.293	0.226	1.556	1.494	1.699
		11.3	15.389	15.459	15.932	15.168	1.712	1.907	0.968	1.080	1.227

The higher the ΔE^* value, the greater the color difference from the initial measurement. Up until measurement (M5-M1), according to Table 3, the samples, in general, presented an increase in the color difference, but this behavior resulted from the application of the inoculum in a liquid medium, which, by moistening the surface of the samples, led to a greater color difference compared with the initial measurement. From (M6-M1), when the lamps are switched on, the samples' surfaces dry up, reducing the values calculated for the ΔE^* . For samples S4, S5, and S6 (with nTiO₂), generally, the ΔE^* increases through (M7-M1) and (M8-M1) (already with an easily visible colony growth) and decreases at (M9-M1) (photoperiod of 4 h/day of UVA light), until (M10-M1), with the lowest ΔE^* values.

Table 4. Luminosity and a* and b* coordinate variation for samples, with and without photocatalyst.

Sample	ΔL^*		Δa^*		Δb^*			
	Sample	(M7-M1)	(M10-M1)	(M7-M1)	(M10-M1)	(M7-M1)	(M10-M1)	
With n TiO ₂	S4	4.1	-2.859	-3.109	-0.637	0.210	-1.380	5.156
		4.2	-0.587	2.002	-0.695	0.276	-1.100	4.691
		4.3	-3.153	0.430	-0.460	0.077	-1.308	2.431
	S5	5.1	-2.114	-0.505	-0.004	0.190	-1.054	1.042
		5.2	-3.177	-2.113	0.046	0.186	-0.834	1.398
		5.3	-1.552	-1.057	-0.027	0.159	-0.962	0.836
	S6	6.1	-2.655	-2.593	-0.614	0.075	-1.568	2.883
		6.2	-2.008	-0.260	-0.442	0.074	-1.167	3.102
		6.3	-4.027	-1.916	-0.235	0.068	-1.181	1.517
Without n TiO ₂	S10	10.1	-0.842	0.457	0.063	-0.192	-3.844	-0.319
		10.2	-0.743	0.814	0.069	-0.241	-3.821	-0.636
		10.3	-0.928	1.187	0.182	-0.104	-3.817	-0.574
	S11	11.1	-4.697	-10.503	-0.546	-0.378	-4.259	1.134
		11.2	0.062	1.492	-0.086	-0.232	-4.215	-0.779
		11.3	-1.756	0.285	-0.272	-0.259	-4.354	-1.165

As for samples S10 and S11, it is probable that the points previously selected for the sample measurements coincided with the growth of the *A. niger* colonies only in S11.1, reaching the maximum ΔE^* value at (M8-M1), and presenting a slight reduction by (M10-M1).

According to Table 4, for the Δa^* values in samples S4, S5, and S6, at (M7-M1) (maximum colony growth), values in the green color scale (-a) were measured, while at (M10-M1), with the maximum reduction of growth, color coordinates in the red scale (+a) were measured. Samples S10 and S11 (without nTiO₂) had Δa^* values mainly in the green color scale (-a). As for the Δb^* values, it was detected that in the samples with nTiO₂, the color measurement alternated from blue (-b) to yellow (+b), while the samples without nTiO₂, in general, presented color coordinates in the blue spectrum (-b) between (M7-M1) and (M10-M1).

Figure 10 shows the behavior of the samples with nTiO₂ (a) and without nTiO₂ (b) regarding ΔE , always in relation to M1, according to the values presented in Table 4.

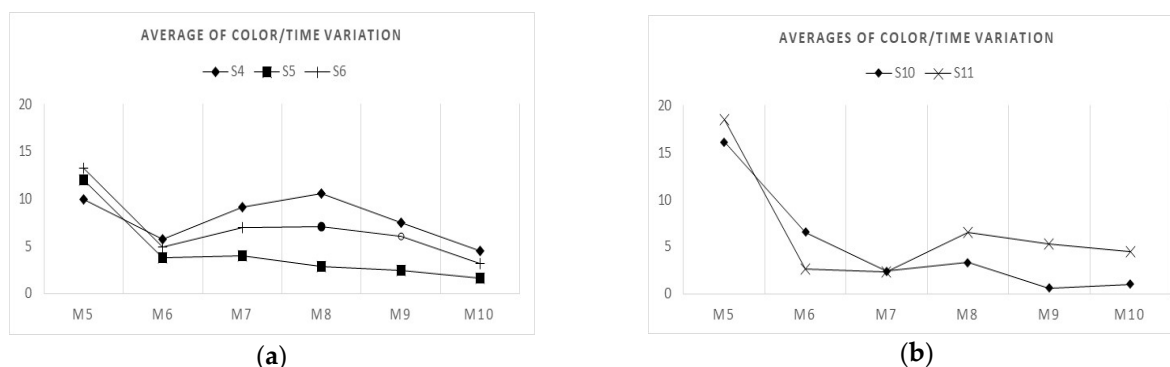
**Figure 10.** ΔE^* over (M5-M1) to (M10-M1) measurement means: (a) with nTiO₂; (b) without nTiO₂.

Figure 11 presents the result of the variance analysis, done with the Statistica 8.0 software [52], for the samples with and without photocatalyst, regarding the growth of *A. niger*, with a 95% confidence interval. A significant difference was detected in the color variation between the samples with photocatalyst, effectively reducing the ΔE between the measurement at greatest fungal growth (M7-M1) and the final measurement (M10-M1). In the samples without the photocatalyst, there was no significant difference in color

variation between the same measurements, indicating that this result is not due only to the application of UVA, but also to the effectiveness of nTiO₂ against *A. niger*.

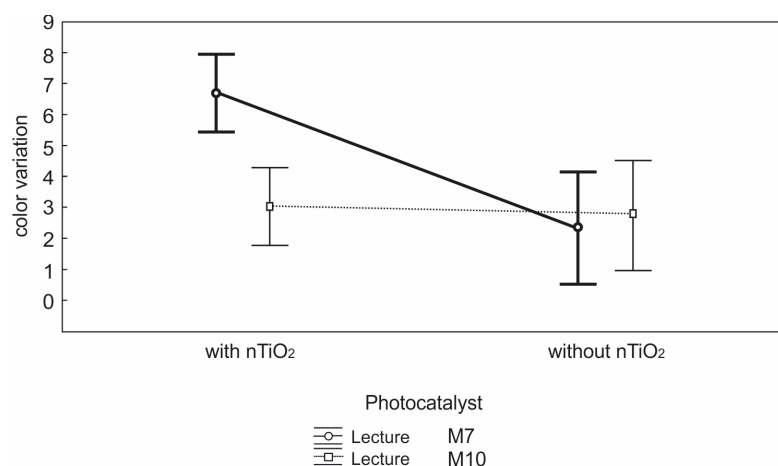


Figure 11. ANOVA (factorial) of the color variation (ΔE) as a function of the application or not of the photocatalyst for *A. niger* (0.95 confidence intervals).

3.3. Image Analyses

Figure S1 in the Supplementary Materials shows the images obtained from sample S4, with the application of nTiO₂. The sequence presents the photo obtained from the sample, the transformation to 8 bits in the gray scale and, lastly, the binarization in black and white pixels, allowing the quantification of the growth area based on the relation between the total of the black pixels and the total sample area. With the aid of a selection tool, it is possible to demarcate the areas to be quantified, corresponding to the fungal growth. It should be noted that the binarization of the images transforms the void areas on the surface of the samples into black pixels, which might distort the quantification, as they do not correspond to the fungal growth. Hence, the use of this tool allowed the exclusive demarcation of the areas pertinent to the quantification, excluding the void areas.

With regards to sample S4, based on Figure S1 (Supplementary Materials), an effective reduction in the staining can be detected. Although the initial staining (M7) corresponds to only 6.06% of the total surface of the sample, in measurement M10, the staining suffered a 100% reduction.

Figure S2 (Supplementary Materials) shows the images of sample S5, with the application of nTiO₂. This sample presented a total staining reduction of 97% of the fungal growth detected between M7 and M10. Sample S6 (Figure S3 in Supplementary Materials) allowed the detection of a staining reduction of 95%.

As for the samples without the application of nTiO₂, the quantification of the staining was done only for sample S11 (Figure S4 in the Supplementary Materials) as it presented the most effective growth of all the samples without the photocatalyst. The difference between measurements M7 and M10 was 41%, showing a small staining reduction when compared with the images with superficial spraying of nTiO₂. Figure S4 in the Supplementary Materials also shows the occurrence of a fungal growth demarcated in the images that probably does not correspond to the *A. niger* fungus. This staining area was excluded from the quantification.

3.4. Images in the Stereoscopic Magnifier

The analysis based on the observation of the biological growth on the samples' surface detected different behaviors in the morphology of the colonies of the *A. niger* isolate, depending on whether the sample had been sprayed with nTiO₂.

In Figure 12, obtained from sample 11, without the application of nTiO₂, it is possible to detect the growth from aerial structures and dark coloration. The hyphae are fine, hyaline, dense, and very ramified, with the presence of white structures deposited on the mycelium, possibly fragments carried by the sample itself.

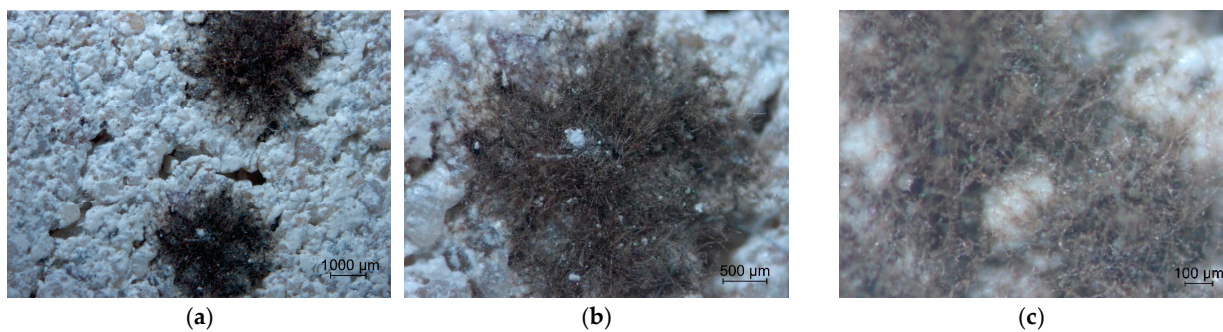


Figure 12. *A. niger* colonies' growth in mortar sample 11 without nTiO₂ application: (a) 1000 μm scale; (b) 500 μm scale; (c) 100 μm scale.

In comparison with Figure 12, Figure 13 shows that in the presence of TiO₂, the structures produced a morphology characterized by greater agglomeration along the samples' surfaces and apparent adherence, without presenting any aerial structures. The observation also allowed the detection of a shiny layer over the entire growth structure. Op De Beeck et al. [53] mention that fungi and bacteria create highly specialized environments around their cells by secreting extracellular polymeric substance matrices (EPS). It is possible that the substance involving the structures visualized through the equipment correspond to the composition of EPS. According to Flemming and Wingender [54], EPS are mainly polysaccharides, proteins, nucleic acids, and lipides. They provide mechanical stability to biofilm and mediate its adhesion to surfaces, forming a cohesive film. Biofilm can act as an external digestive system, keeping extracellular enzymes close to the cells, allowing them to metabolize dissolved, colloidal, and solid biopolymers.

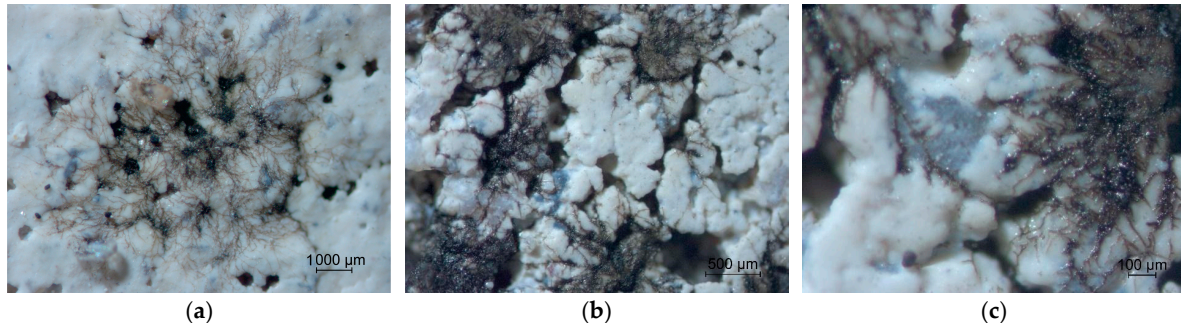


Figure 13. *A. niger* colonies' growth in mortar sample 4 with nTiO₂ application: (a) 1000 μm scale; (b) 500 μm scale; (c) 100 μm scale.

Considering the conditions of the presence or absence of nTiO₂ in the samples, the probable morphology of the biofilm may have resulted in the strongly adhered and coated aspect of this shiny film, as a reaction of the growing colonies to an environment unfavorable to their maintenance due to the presence of the photocatalyst, which is evidence of a possible stress situation and an effort towards environmental adaptation for biological survival.

Sun et al. [55] highlight that *A. fungi* produce a rich extracellular matrix consisting of polysaccharides, melanin, and other compounds, with the aim of protecting the mycelium from adverse external factors, including oxidative stress. The same authors point out that the *A. niger* fungus intensely produces melanin as a protective layer for the mycelium when under light illumination. Considering the importance of melanin production in the formation of biofilm, the experiment in this study showed that the colonies presented a different growth behavior when nTiO₂ was activated. That indicates that the production of oxidative radicals resulting from photocatalysis, in joint action with the incidence of light, induced greater production of melanin because of the stress caused by the action of the photocatalyst.

In relation to historic buildings, having verified their efficiency against the development of the fungi capable of causing changes in the mortars of these buildings, the evaluation of simple ways of applying the photocatalyst, including in interior environments, is relevant and of great interest to the professionals responsible for the conservation of these buildings. To La Russa et al. [29], TiO₂ is characterized by chemical stability, non-toxicity, high photoreactivity, antibiosis and low cost, and has been widely used as a biocide against various microorganisms as bacteria, fungi, and viruses. The limitation in the use is due its reactivity in a restricted wavelength in the UV region, and therefore, its application may be limited in certain circumstances (for example, indoors). Recently, alkaline earth metal ions have been considered promising, efficient, and economical approaches to doping TiO₂, as they have a larger photocatalytic spectrum.

Our study was initially based on effectiveness in relation to the proposed mortar substrate, for an isolate of fungus that recurs in historic Brazilian buildings. New analyses are being conducted to adapt the study conditions to the selected sample.

Finally, this work did not evaluate the mechanisms of interaction between the photocatalysis and the fungus investigated, resulting in the regression of the stain surface, probably due to cell death. Photocatalysis is characterized as an advanced oxidative process (AOP), presenting diverse applications due to the generation of strong oxidizing species. According to La Russa et al. [29], efficiency in relation to microorganisms is related to the competition between the recombination (nanoseconds) of photo-excited charges and electrons and their transfer to the interior of the cells. According to Mitoraj et al. and Ilkhechi et al. [56,57], the mechanism for the antifungal activity of photocatalytic compounds may be based on the formation of high levels of reactive oxygen species (ROS) that disrupt the integrity of the fungal cell membrane, which aids in the damage of microbial enzyme bodies, thus killing the fungi. The interaction between the photocatalysis reaction and fungal cells has not yet been sufficiently investigated, although several studies report fungal cell death when interacting with the TiO₂ photocatalyst, including the fungus *A. niger* under analysis in this study. According Mitoraj et al. [57], there is a direct dependency between increasing the formation of reactive oxygen species (ROS) and the fungicide of nanoparticles.

4. Conclusions

Based on the analyses presented, and considering the adopted conditions of study, it is possible to conclude that:

- When performing controlled tests in Biological Oxygen Demand (BOD), it is crucially important to control the RH and the temperature as to minimum, medium, and maximum values for spore germination and growth of the mycelium of the fungal isolate under investigation, so as to allow its adequate growth and the subsequent evaluation of the effectiveness of the photocatalyst under study;
- Although the spectrophotometer readings are efficient at quantitatively determining the color variation and luminosity of the samples over time, they are still limited when it is necessary to predetermine the reading points, since fungal growth occurs in a non-uniform/heterogenous manner, according to the samples' surface features;
- The readings performed with the spectrophotometer allowed the verification of effectiveness of nTiO₂ against the *A. niger* fungus regarding reduction of growth and clearing the staining on mortar samples exposed to UVA light with a daily photoperiod of 4 h during seven months, after the colonies' growth had been established; however, considering the reduced number of samples, more studies may help confirm the behavior;
- The quantification of the reduction in the staining area through counting the number of pixels in the samples' images showed there was a reduction of up to 100% in the staining in the samples sprayed with nTiO₂;
- It was observed that the previous application of nTiO₂ on the mortar samples may have been responsible for alterations in the morphology of the *A. niger* fungus struc-

tures, evidence of a disturbance in the growth of the colonies or even their reduction over time.

Supplementary Materials: The following supporting information can be downloaded at: <https://www.mdpi.com/article/10.3390/buildings13112751/s1>, Figure S1: percentage of staining in sample 4 with TiO₂: (a) JPEG image format, (b) image in gray scale, (c) binarized image (black and white pixels), (d) demarcation of the quantified area in red, Figure S2: percentage of staining in sample 5 with TiO₂: (a) JPEG image format, (b) image in gray scale, (c) binarized image (black and white pixels), (d) demarcation of the quantified area in red, Figure S3: percentage of staining in the sample 6 with TiO₂: (a) JPEG image format, (b) image in gray scale, (c) binarized image (black and white pixels), (d) demarcation of the quantified area in red, Figure S4: percentage of staining in the sample 11 without TiO₂: (a) JPEG image format, (b) image in gray scale, (c) binarized image (black and white pixels), (d) demarcation of the quantified area in red.

Author Contributions: Conceptualization, F.L.G., A.B.M. and D.C.C.D.M.; methodology, F.L.G., A.B.M., D.C.C.D.M. and F.M.B.; software, F.L.G. and C.G.; validation, F.L.G., A.B.M., D.C.C.D.M. and F.M.B.; formal analysis, F.L.G., C.G., R.R. and L.Z.; investigation, F.L.G., C.G., L.Z. and R.R.; resources, A.B.M., D.C.C.D.M. and F.M.B.; writing—original draft preparation, F.L.G.; writing—review and editing, F.L.G., A.B.M., D.C.C.D.M., F.M.B., C.G., L.Z. and R.R.; visualization, F.L.G.; supervision, A.B.M., D.C.C.D.M. and F.M.B.; All authors have read and agreed to the published version of the manuscript.

Funding: This research was funded by CNPq (Conselho Nacional de Desenvolvimento Científico e Tecnológico), grant number 141775/2018-1 and CAPES (coordenação de Aperfeiçoamento de Pessoal de Nível Superior), grant number 88882.316356/2019-01.

Data Availability Statement: Not applicable.

Acknowledgments: The authors appreciate the support of LAMTAC (Laboratório de Materiais e Tecnologia do Ambiente Construído), PPGCI (Programa de Pós-Graduação em Engenharia Civil: Construção e Infraestrutura), LAB-BIO (Laboratório de Biodeterioração de Combustíveis e Biocombustíveis), ICBS (Instituto de Ciências Básicas da Saúde, CBIOT (Centro de Biotecnologia), and UFRGS (Universidade Federal do Rio Grande do Sul).

Conflicts of Interest: The authors declare no conflict of interest. The funders had no role in the design of the study; in the collection, analyses, or interpretation of data; in the writing of the manuscript; or in the decision to publish the results.

References

1. Arioglu, N.; Acun, S.Ā. A Research about a Method for Restoration of Traditional Lime Mortars and Plasters: A Staging System Approach. *Build. Environ.* **2006**, *41*, 1223–1230. [[CrossRef](#)]
2. Veniale, F.; Setti, M.; Lodola, S. Diagnosing Stone Decay in Built Heritage. Facts and Perspectives. *Mater. Constr.* **2008**, *58*, 11–32. [[CrossRef](#)]
3. Loureiro, A.M.S.; da Paz, S.P.A.; do Rosário Veiga, M.; Angélica, R.S. Investigation of Historical Mortars from Belém Do Pará, Northern Brazil. *Constr. Build. Mater.* **2020**, *233*, 117284. [[CrossRef](#)]
4. Sena da Fonseca, B.; Ferreira Pinto, A.P.; Vaz Silva, D. Compositional and Textural Characterization of Historical Bedding Mortars from Rubble Stone Masonries: Contribution for the Design of Compatible Repair Mortars. *Constr. Build. Mater.* **2020**, *247*, 118627. [[CrossRef](#)]
5. Ponce-Antón, G.; Arizzi, A.; Zuluaga, M.C.; Cultrone, G.; Ortega, L.A.; Mauleon, J.A. Mineralogical, Textural and Physical Characterisation to Determine Deterioration Susceptibility of Irulegi Castle Lime Mortars (Navarre, Spain). *Materials* **2019**, *12*, 584. [[CrossRef](#)] [[PubMed](#)]
6. Garg, K.L.; Jain, K.K.; Mishra, A.K. Role of Fungi in the Deterioration of Wall Paintings. *Sci. Total Environ.* **1995**, *167*, 255–271. [[CrossRef](#)]
7. Rodríguez-González, V.; Obregón, S.; Patrón-Soberano, O.A.; Terashima, C.; Fujishima, A. An Approach to the Photocatalytic Mechanism in the TiO₂-Nanomaterials Microorganism Interface for the Control of Infectious Processes. *Int. Biodeterior. Biodegrad.* **2020**, *270*, 118853. [[CrossRef](#)]
8. Kirthika, S.K.; Goel, G.; Matthews, A.; Goel, S. Review of the Untapped Potentials of Antimicrobial Materials in the Construction Sector. *Prog. Mater. Sci.* **2023**, *133*, 101065. [[CrossRef](#)]
9. Jiang, L.; Pettitt, T.R.; Buenfeld, N.; Smith, S.R. A Critical Review of the Physiological, Ecological, Physical and Chemical Factors Influencing the Microbial Degradation of Concrete by Fungi. *Build. Environ.* **2022**, *214*, 108925. [[CrossRef](#)]

10. Beimforde, C. Biodeterioration (of Stone). In *Encyclopedia of Geobiology*; Reitner, J., Thiel, V., Eds.; Springer: Dordrecht, The Netherlands, 2011; pp. 112–117. [[CrossRef](#)]
11. Harding, M.W.; Marques, L.L.R.; Howard, R.J.; Olson, M.E. Can Filamentous Fungi Form Biofilms? *Trends Microbiol.* **2009**, *17*, 475–480. [[CrossRef](#)]
12. Burford, E.P.; Fomina, M.; Gadd, G.M. Fungal Involvement in Bioweathering and Biotransformation of Rocks and Minerals. *Mineral. Mag.* **2003**, *67*, 1127–1155. [[CrossRef](#)]
13. Verrecchia, E. Pedogenic Carbonates. In *Encyclopedia of Geobiology*; Reitner, J., Thiel, V., Eds.; Springer: Dordrecht, The Netherlands, 2011; pp. 721–725. [[CrossRef](#)]
14. Borrego, S.; Guimet, P.; Gómez, S.; Saravia, D.; Batistini, P.; Garcia, M.; Lavin, P.; Perdomo, I. The Quality of Air at Archives and the Biodeterioration of Photographs. *Int. Biodeterior. Biodegrad.* **2010**, *64*, 139–145. [[CrossRef](#)]
15. Wei, S.; Jiang, Z.; Liu, H.; Zhou, D.; Sanchez-Silva, M. Microbiologically Induced Deterioration of Concrete: A Review. *Braz. J. Microbiol.* **2013**, *44*, 1001–1007. [[CrossRef](#)] [[PubMed](#)]
16. Coffin, M.; Lent, T.; Sabella, S.; Vallette, J.; Walsh, B.; Dickinson, M.; Drake, S.; Guenther, R.; Richter, M. Understanding Antimicrobial Ingredients in Building Materials. 2017. Available online: <https://healthybuilding.net/reports/4-healthy-environments-understanding-antimicrobial-ingredients-in-building-materials> (accessed on 30 October 2023).
17. Liu, G.; Li, G.; Qiu, X.; Li, L. Synthesis of ZnO/Titanate Nanocomposites with Highly Photocatalytic Activity under Visible Light Irradiation. *J. Alloys Compd.* **2009**, *481*, 492–497. [[CrossRef](#)]
18. Dei, L.; Salvadori, B. Nanotechnology in Cultural Heritage Conservation: Nanometric Slaked Lime Saves Architectonic and Artistic Surfaces from Decay. *J. Cult. Herit.* **2006**, *7*, 110–115. [[CrossRef](#)]
19. Paramés, J.R.R. Nanotecnologias Na Indústria Da Construção. Master's Thesis, Universidade Técnica de Lisboa, Lisboa, Portugal, 2008.
20. Ruffolo, S.A.; La Russa, M.F.; Malagodi, M.; Oliviero Rossi, C.; Palermo, A.M.; Crisci, G.M. ZnO and ZnTiO₃ Nanopowders for Antimicrobial Stone Coating. *Appl. Phys. A Mater. Sci. Process.* **2010**, *100*, 829–834. [[CrossRef](#)]
21. Di Simoni, I. Nanomateriali per Il Restauro Architettonico: Stato Dell'arte e Prospettive. Bachelor's Thesis, Università di Bologna, Bologna, Italia, 2012.
22. Gutarowska, B.; Skora, J.; Zduniak, K.; Rembisz, D. Analysis of the Sensitivity of Microorganisms Contaminating Museums and Archives to Silver Nanoparticles. *Int. Biodeterior. Biodegrad.* **2012**, *68*, 7–17. [[CrossRef](#)]
23. Lucas, S.S.; Ferreira, V.M.; De Aguiar, J.L.B. Incorporation of Titanium Dioxide Nanoparticles in Mortars—Influence of Microstructure in the Hardened State Properties and Photocatalytic Activity. *Cem. Concr. Res.* **2013**, *43*, 112–120. [[CrossRef](#)]
24. Shirakawa, M.A.; Werle, A.P.; Gaylarde, C.C.; Loh, K.; John, V. Effect of Microbial Growth on Reflectance of Roofing Tiles. In Proceedings of the Biodeterioration & Biodegradation in Latin America LABS 8; Bento, F.M., Hidalgo, G.E.N., Gaylarde, C.C., Shirakawa, M.A., Camargo, F.A.O., Eds.; Editora Evangraf Ltda.: Porto Alegre, Brazil, 2014; pp. 10–13.
25. Munafò, P.; Quagliarini, E.; Goffredo, G.B.; Bondioli, F.; Licciulli, A. Durability of Nano-Engineered TiO₂ Self-Cleaning Treatments on Limestone. *Constr. Build. Mater.* **2014**, *65*, 218–231. [[CrossRef](#)]
26. Calia, A.; Lettieri, M.; Masieri, M. Durability Assessment of Nanostructured TiO₂ Coatings Applied on Limestones to Enhance Building Surface with Self-Cleaning Ability. *Build. Environ.* **2016**, *110*, 1–10. [[CrossRef](#)]
27. Fujishima, A.; Zhang, X.; Tryk, D.A. TiO₂ Photocatalysis and Related Surface Phenomena. *Surf. Sci. Rep.* **2008**, *63*, 515–582. [[CrossRef](#)]
28. Pozo-Antonio, J.S.; Dionísio, A. Physical-Mechanical Properties of Mortars with Addition of TiO₂ Nanoparticles. *Constr. Build. Mater.* **2017**, *148*, 261–272. [[CrossRef](#)]
29. La Russa, M.F.; Macchia, A.; Ruffolo, S.A.; De Leo, F.; Barberio, M.; Barone, P.; Crisci, G.M.; Urzì, C. Testing the Antibacterial Activity of Doped TiO₂ for Preventing Biodeterioration of Cultural Heritage Building Materials. *Int. Biodeterior. Biodegrad.* **2014**, *96*, 87–96. [[CrossRef](#)]
30. Janczarek, M.; Klapiszewski, Ł.; Jędrzejczak, P.; Klapiszewska, I.; Ślosarczyk, A.; Jesionowski, T. Progress of Functionalized TiO₂-Based Nanomaterials in the Construction Industry: A Comprehensive Review. *Chem. Eng. J.* **2022**, *430*, 132062. [[CrossRef](#)]
31. Casarin, R.P.; Bersch, J.D.; Maia, J.; Masuero, A.B.; Dal Molin, D.C.C. Assessment of Photocatalytic Nano-TiO₂ Mortars' Behavior When Exposed to Simulated Indoor Conditions of Glazed Buildings. *Buildings* **2023**, *13*, 2250. [[CrossRef](#)]
32. Jędrzejczak, P.; Janczarek, M.; Parus, A.; Gapiński, B.; Hotěk, P.; Fiala, L.; Jesionowski, T.; Ślosarczyk, A.; Černý, R.; Klapiszewski, Ł. Carbon-Modified TiO₂ as a Promising and Efficient Admixture for Cementitious Composites: A Comprehensive Study of Photocatalytic, Mechanical and Structural Properties. *J. Build. Eng.* **2023**, *78*, 107747. [[CrossRef](#)]
33. Castro-Hoyos, A.M.; Rojas Manzano, M.A.; Maury-Ramírez, A. Challenges and Opportunities of Using Titanium Dioxide Photocatalysis on Cement-Based Materials. *Coatings* **2022**, *12*, 968. [[CrossRef](#)]
34. Guerra, F.L.; Lopes, W.; Cazarolli, J.C.; Lobato, M.; Masuero, A.B.; Dal Molin, D.C.C.; Bento, F.M.; Schrank, A.; Vainstein, M.H. Biodeterioration of Mortar Coating in Historical Buildings: Microclimatic Characterization, Material, and Fungal Community. *Build. Environ.* **2019**, *155*, 195–209. [[CrossRef](#)]
35. Kaur, S.; Singh, S. Biofilm Formation by *Aspergillus Fumigatus*. *Med. Mycol.* **2014**, *52*, 2–9. [[CrossRef](#)] [[PubMed](#)]
36. NBR 13276; Argamassa Para Assentamento e Revestimento de Paredes e Tetos—Determinação Do Índice de Consistência. Associação Brasileira de Normas Técnicas: Rio de Janeiro, Brazil, 2016.

37. NBR 13278; Argamassa Para Assentamento e Revestimento de Paredes e Tetos Determinação da Densidade de Massa e Do Teor de Ar Incorporado. Associação Brasileira de Normas Técnicas: Rio de Janeiro, Brazil, 2005.
38. NBR 13279; Argamassa Para Assentamento e Revestimento de Paredes e Tetos Determinação Da Resistência à Tração Na Flexão e à Compressão. Associação Brasileira de Normas Técnicas: Rio de Janeiro, Brazil, 2005.
39. NBR 15259; Argamassa Para Assentamento e Revestimento de Paredes e Tetos Determinação da Absorção de Água Por Capilaridade e Do Coeficiente de Capilaridade. Associação Brasileira de Normas Técnicas: Rio de Janeiro, Brazil, 2005.
40. NBR 15630; Argamassa Para Assentamento e Revestimento de Paredes e Tetos—Determinação Do Módulo de Elasticidade Dinâmico Através da Propagação de Onda Ultra-Sônica. Associação Brasileira de Normas Técnicas: Rio de Janeiro, Brazil, 2008.
41. NBR 13280; Argamassa Para Assentamento e Revestimento de Paredes e Tetos Determinação da Densidade de Massa Aparente No Estado Endurecido. Associação Brasileira de Normas Técnicas: Rio de Janeiro, Brazil, 2005.
42. Shirakawa, M.A.; Cincotto, M.A.; Gambale, W. Padronização de Teste Acelerado Para a Avaliação Da Resistência de Argamassas de Revestimento de Interiores Ao Crescimento de Fungos. In Proceedings of the III Simpósio Brasileiro de Tecnologia das Argamassas, Vitória, Brazil, 22–23 April 1999.
43. Shirakawa, M.A.; Beech, I.B.; Tapper, R.; Cincotto, M.A.; Gambale, W. The Development of a Method to Evaluate Bioreceptivity of Indoor Mortar Plastering to Fungal Growth. *Int. Biodeterior. Biodegrad.* **2003**, *51*, 83–92. [[CrossRef](#)]
44. Austria, G. Argamassa Autolimpante Para Revestimento de Fachadas: O Efeito Das Propriedades Fotocatalíticas Do Dióxido de Titânio (TiO₂). Master's Thesis, Universidade Federal do Rio Grande do Sul (UFRGS), Porto Alegre, Brazil, 2015.
45. Gherardi, F.; Colombo, A.; Goidanich, S.; Simonutti, R.; Toniolo, L. Innovative Nano-TiO₂ Particles for Self-Cleaning Treatments of Historic Architecture and Sculptures. In Proceedings of the Hydrophobe VII: 7th International Conference on Water Repellent Treatment and Protective Surface Technology for Building Materials, Lisboa, Portugal, 11–12 September 2014; Charola, A.E., Rodrigues, J.D., Eds.; pp. 205–214.
46. Goffredo, G.B.; Accoroni, S.; Totti, C.; Romagnoli, T.; Valentini, L.; Munafò, P. Titanium Dioxide Based Nanotreatments to Inhibit Microalgal Fouling on Building Stones Surfaces. *Build. Environ.* **2016**, *112*, 209–222. [[CrossRef](#)]
47. Treviso, J.P. Avaliação Da Eficiência de Autolimpeza Em Argamassas e Pastas Contendo TiO₂ Expostas Ao Microclima Urbano. Master's Thesis, Universidade Federal do Rio Grande do Sul (UFRGS), Porto Alegre, Brazil, 2016.
48. Vázquez-Nion, D.; Silva, B.; Prieto, B. Influence of the Properties of Granitic Rocks on Their Bioreceptivity to Subaerial Phototrophic Biofilms. *Sci. Total Environ.* **2018**, *610–611*, 44–54. [[CrossRef](#)] [[PubMed](#)]
49. Ruot, B.; Plassais, A.; Olive, F.; Guillot, L.; Bonafous, L. TiO₂-Containing Cement Pastes and Mortars: Measurements of the Photocatalytic Efficiency Using a Rhodamine B-Based Colourimetric Test. *Sol. Energy* **2009**, *83*, 1794–1801. [[CrossRef](#)]
50. Schneider, C.A.; Rasband, W.S.; Eliceiri, K.W. NIH Image to ImageJ: 25 Years of Image Analysis. *Nat. Methods* **2012**, *9*, 671–675. [[CrossRef](#)]
51. Sedlbauer, K. Prediction of Mould Growth by Hygrothermal Calculation. *J. Therm. Envel. Build. Sci.* **2002**, *25*, 321–336. [[CrossRef](#)]
52. StatSoft, Inc. *Statistica (Data Analysis Software System)*, 8th ed.; Statsoft Inc.: Tulsa, OK, USA, 2007.
53. Op De Beeck, M.; Persson, P.; Tunlid, A. Fungal Extracellular Polymeric Substance Matrices—Highly Specialized Microenvironments That Allow Fungi to Control Soil Organic Matter Decomposition Reactions. *Soil. Biol. Biochem.* **2021**, *159*, 108304. [[CrossRef](#)]
54. Flemming, H.C.; Wingender, J. The Biofilm Matrix. *Nat. Rev. Microbiol.* **2010**, *8*, 623–633. [[CrossRef](#)]
55. Sun, W.; Yu, Y.; Chen, J.; Yu, B.; Chen, T.; Ying, H.; Zhou, S.; Ouyang, P.; Liu, D.; Chen, Y. Light Signaling Regulates Aspergillus Niger Biofilm Formation by Affecting Melanin and Extracellular Polysaccharide Biosynthesis. *mBio* **2021**, *12*, e03434-20. [[CrossRef](#)]
56. Najibi Ilkhechi, N.; Mozammel, M.; Yari Khosroushahi, A. Antifungal Effects of ZnO, TiO₂ and ZnO-TiO₂ Nanostructures on Aspergillus Flavus. *Pestic. Biochem. Physiol.* **2021**, *176*, 104869. [[CrossRef](#)]
57. Mitoraj, D.; Jańczyk, A.; Strus, M.; Kisch, H.; Stochel, G.; Heczko, P.B.; Macyk, W. Visible Light Inactivation of Bacteria and Fungi by Modified Titanium Dioxide. *Photochem. Photobiol. Sci.* **2007**, *6*, 642–648. [[CrossRef](#)]

Disclaimer/Publisher's Note: The statements, opinions and data contained in all publications are solely those of the individual author(s) and contributor(s) and not of MDPI and/or the editor(s). MDPI and/or the editor(s) disclaim responsibility for any injury to people or property resulting from any ideas, methods, instructions or products referred to in the content.